PNAS RESEARCH ARTICLE | MICROBIOLOGY
BIOPHYSICS AND COMPUTATIONAL BIOLOGY OPEN ACCESS

Dispensability of extrinsic DnaA regulators in *Escherichia coli* cell-cycle control

Thias Oberg Boesen[a,1], Godefroid Charbon[a,1], Haochen Fu[b,1], Cara Jensen[b], Michael Sandler[b], Suckjoon Jun[b,2], and Anders Løbner-Olesen[a,2]

Affiliations are included on p. 9.

Edited by Susan Lovett, Brandeis University, Waltham, MA; received December 28, 2023; accepted June 26, 2024

Investigating a long-standing conceptual question in bacterial physiology, we examine why DnaA, the bacterial master replication initiator protein, exists in both ATP and ADP forms, despite only the ATP form being essential for initiation. We engineered the Δ4 *Escherichia coli* strain, devoid of all known external elements facilitating the DnaA-ATP/ADP conversion and found that these cells display nearly wild-type behaviors under nonoverlapping replication cycles. However, during rapid growth with overlapping cycles, Δ4 cells exhibit initiation instability. This aligns with our model predictions, suggesting that the intrinsic ATPase activity of DnaA alone is sufficient for robust initiation control in *E. coli* and the DnaA-ATP/ADP conversion regulatory elements extend the robustness to multifork replication, indicating an evolutionary adaptation. Moreover, our experiments revealed constant DnaA concentrations during steady-state cell elongation in both wild-type and Δ4 cells. These insights not only advance our understanding of bacterial cell-cycle regulation and DnaA but also highlight a fundamental divergence from eukaryotic cell-cycle controls, emphasizing protein copy-number sensing in bacteria versus programmed protein concentration oscillations in eukaryotes.

replication initiation | bacterial physiology | DnaA | quantitative biology

Significance

This study addresses a long-standing question in bacterial physiology on why the master initiator protein in bacteria exists in two forms, DnaA-ATP and DnaA-ADP. We show that the Δ4 *Escherichia coli*, the engineered strain with all four extrinsic regulatory elements facilitating DnaA-ATP/ADP conversion removed, can behave surprisingly normally. Thus, the intrinsic ATPase activity of DnaA alone can be sufficient for viability. However, the conversion elements enhance replication robustness during overlapping replication cycles unique to bacteria, indicating an evolutionary adaptation. Additionally, our findings reveal a near-constant DnaA concentration during cell elongation in both wild-type and Δ4 *E. coli*. This provides a critical insight into bacterial cell-cycle regulation and underscores its fundamental difference from eukaryotic cell-cycle controls.

Initiation of chromosome replication in bacteria is a highly regulated process, intricately linked with cellular growth and division. This precision is evident in the remarkably consistent cell size at initiation observed in *Escherichia coli* and *Bacillus subtilis*, with a coefficient of variation (CV) of no more than 10%—notably lower than other physiological variables with CVs around 20% (1–5). These bacteria maintain a stable initiation mass (the cell size per origin) across various growth conditions, exemplified by *E. coli*'s initiation mass varying by a maximum of 20% over a 10-fold growth rate range (5–8).

The molecular biology of initiation in *E. coli* has been extensively studied, particularly focusing on its master regulator, DnaA (9–11). Replication begins at the origin *oriC*, initiated by DnaA binding. DnaA functions as an AAA+ ATPase, existing in either an active (DnaA-ATP) or inactive (DnaA-ADP) form (12). The *oriC* region contains both high- and low-affinity binding sites for the two forms of DnaA (13). Though the high-affinity binding sites have similar binding affinities for both DnaA-ATP and DnaA-ADP (12), only DnaA-ATP can bind the low-binding sites helped by cooperativity (14, 15). Prior to initiation, the high-affinity DnaA boxes are occupied by either DnaA-ATP or DnaA-ADP (16, 17) while the nucleoid-associated protein (NAP) Fis is bound to its recognition sequence (18, 19). Initiation commences with formation of a DnaA-ATP filament on the low-affinity binding sites in the right half of *oriC*, which displaces Fis and allows another NAP, IHF, to bind its recognition sequence in the left half of *oriC* (20). IHF binding allows for formation of a second DnaA-ATP filament on the low-affinity binding sites in the left half of *oriC*. This generates the tension that opens the duplex at the adjacent DUE site (21), facilitating replisome assembly (12, 22–24). This mechanism underscores the necessity of DnaA-ATP for initiation.

Several factors influencing the DnaA-ADP ↔ DnaA-ATP conversion have been identified. DARS1 and DARS2 (DnaA rejuvenating sequences 1 and 2) facilitate the conversion from DnaA-ADP to DnaA-ATP, while RIDA (regulatory inactivation of DnaA) and DDAH (*datA*-dependent DnaA-ATP hydrolysis) mechanisms promote the reverse conversion (25–27). These elements' perturbations impact initiation precision and synchrony to varying degrees (28–30).

Despite these discoveries, the role of DnaA-ADP on initiation control has been one of the least understood. A natural hypothesis is that the DnaA-ADP ↔ DnaA-ATP conversion creates periodic oscillations in their concentrations, with replication initiating when the ratio of [DnaA-ATP]/[DnaA-ADP] peaks (31–33). By contrast, the notion of

Author contributions: T.O.B., G.C., H.F., S.J., and A.L.-O. designed research; T.O.B., G.C., H.F., C.J., M.S., and S.J. performed research; T.O.B., G.C., H.F., C.J., and S.J. analyzed data; and T.O.B., H.F., S.J., and A.L.-O. wrote the paper.

The authors declare no competing interest.

This article is a PNAS Direct Submission.

[1]T.O.B., G.C., and H.F. contributed equally to this work.

[2]To whom correspondence may be addressed. Email: suckjoon.jun@gmail.com or lobner@bio.ku.dk.

This article contains supporting information online at https://www.pnas.org/lookup/suppl/doi:10.1073/pnas.2322772121/-/DCSupplemental.

Published August 6, 2024.

balanced biosynthesis has been one of the foundations of bacterial physiology since the 1950s, which states that the average synthesis rate of biomolecules inside the cell is the same as the growth rate of the cells (34, 35). As a consequence, the concentration of cell cycle initiators is maintained nearly constant during cell elongation (1). Therefore, control of the cell cycle based on the oscillation of an initiator concentration must be reconciled with the concept of balanced growth in bacteria.

Building upon the initiator titration model (36), we previously proposed that DnaA-ADP is not required for initiation but helps stabilize it by preventing reinitiations (33). Here, we show that DnaA's intrinsic ATPase activity alone can be sufficient for precise and robust initiation in *E. coli*. We created the "Δ4" *E. coli* strain, devoid of all known external DnaA-ADP ↔ DnaA-ATP conversion elements. This strain not only survives but also exhibits near wild-type behavior under nonoverlapping replication cycles. We also address how the extrinsic DnaA-ADP ↔ DnaA-ATP conversion elements can stabilize replication initiation in overlapping replication cycles, aligning with recent model predictions by us and others (32, 33). Additionally, our single-cell level analysis reveals near-balanced DnaA synthesis, revealing that *dnaA* promoter's autorepression or sequestration only marginally impacts the DnaA concentration during cell elongation. These findings offer insights into bacterial cell cycle control, its evolutionary aspects, and fundamental distinctions from eukaryotic mechanisms.

Results

DnaA-ATP ↔ DnaA-ADP Conversion and Construction of the $\Delta 2^{ATP}$ and $\Delta 2^{ADP}$ *E. coli* Cells. Currently, four extrinsic factors for the DnaA-ADP ↔ DnaA-ATP conversion are known (Fig. 1*A*). For DnaA-ADP → DnaA-ATP, DARS1 and DARS2 at different loci on the chromosome have been characterized (26, 37, 38). For DnaA-ATP → DnaA-ADP, the two extrinsic mechanisms are RIDA mediated by Hda and the DNA-loaded β-sliding clamps (25, 39–42), and DDAH mediated at the five DnaA boxes at the *datA* locus (27, 29).

To examine the impact of the extrinsic DnaA-ADP → DnaA-ATP vs. DnaA-ATP → DnaA-ADP regulatory elements on initiation, we constructed two types of *E. coli* strains: $\Delta 2^{ATP}$ (ΔDARS1 and ΔDARS2) and $\Delta 2^{ADP}$ (Δ*hda* + Δ*datA*) strains. Therefore, in the $\Delta 2^{ATP}$ cells, the only source of DnaA-ATP is the de novo synthesis of DnaA, which becomes DnaA-ATP due to the high cytoplasmic ATP concentration. By contrast, the $\Delta 2^{ADP}$ cells must exclusively rely on the intrinsic ATPase activity of DnaA to convert DnaA-ATP to DnaA-ADP. Consequently, the $\Delta 2^{ATP}$ cells should have lower [DnaA-ATP] and DnaA-ATP/DnaA-ADP ratio than the wild-type cells, whereas the $\Delta 2^{ADP}$ cells must exhibit a higher level of DnaA-ATP and the DnaA-ATP/DnaA-ADP ratio. See the section below, "DnaA-ATP/DnaA-ADP ratio and *dnaA* promoter activity in wild-type, Δ2, and Δ4 *E. coli*."

DnaA-ATP → DnaA-ADP and DnaA-ADP → DnaA-ATP Have Opposing Effects on Initiation. One of the main goals of the present study is to differentiate the impact of initiation mutants on initiation and the role of DnaA-ATP ↔ DnaA-ADP conversion. For example, wild-type cells generally show highly synchronized initiation (Fig. 1*C*), even when the initiation mass can vary significantly from cell to cell.

The single-cell initiation data show stark differences between $\Delta 2^{ATP}$ vs. $\Delta 2^{ADP}$ cells (Fig. 2). First, $\Delta 2^{ATP}$ exhibits a notable

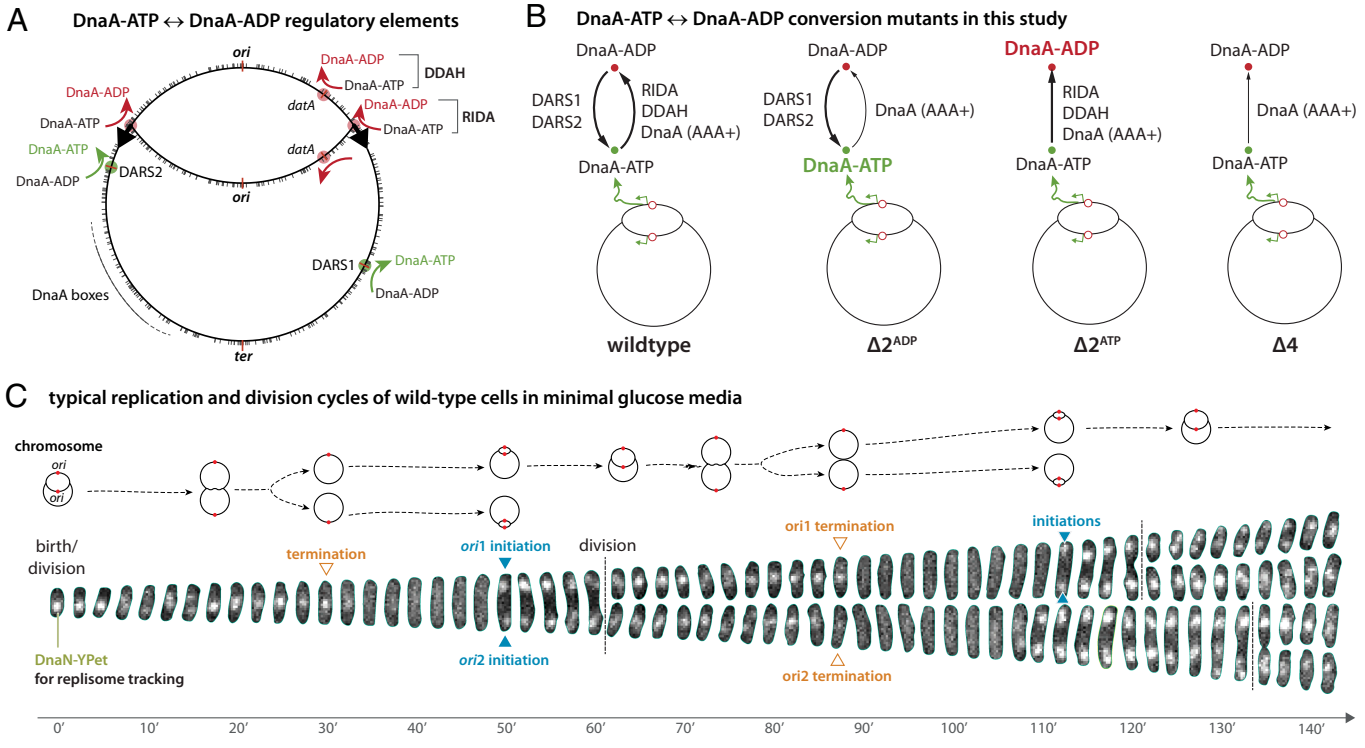

Fig. 1. Extrinsic DnaA-ATP ↔ DnaA-ADP conversion elements. (*A*) The four extrinsic DnaA-ATP ↔ DnaA-ADP conversion regulatory elements. (*B*) We constructed $\Delta 2^{ATP}$ (ΔDARS1 ΔDARS2), $\Delta 2^{ADP}$ (Δ*hda* Δ*datA*), and Δ4 (ΔDARS1 ΔDARS2 Δ*hda* Δ*datA*) *E. coli* strains. (*C*) Tracking the replication dynamics using fluorescence-labeled replisomes (DnaN-YPet) (1) (*Materials and Methods*). Chromosome configurations (tracking only the top cells) over time are shown above. The wild-type cells typically initiate synchronously.

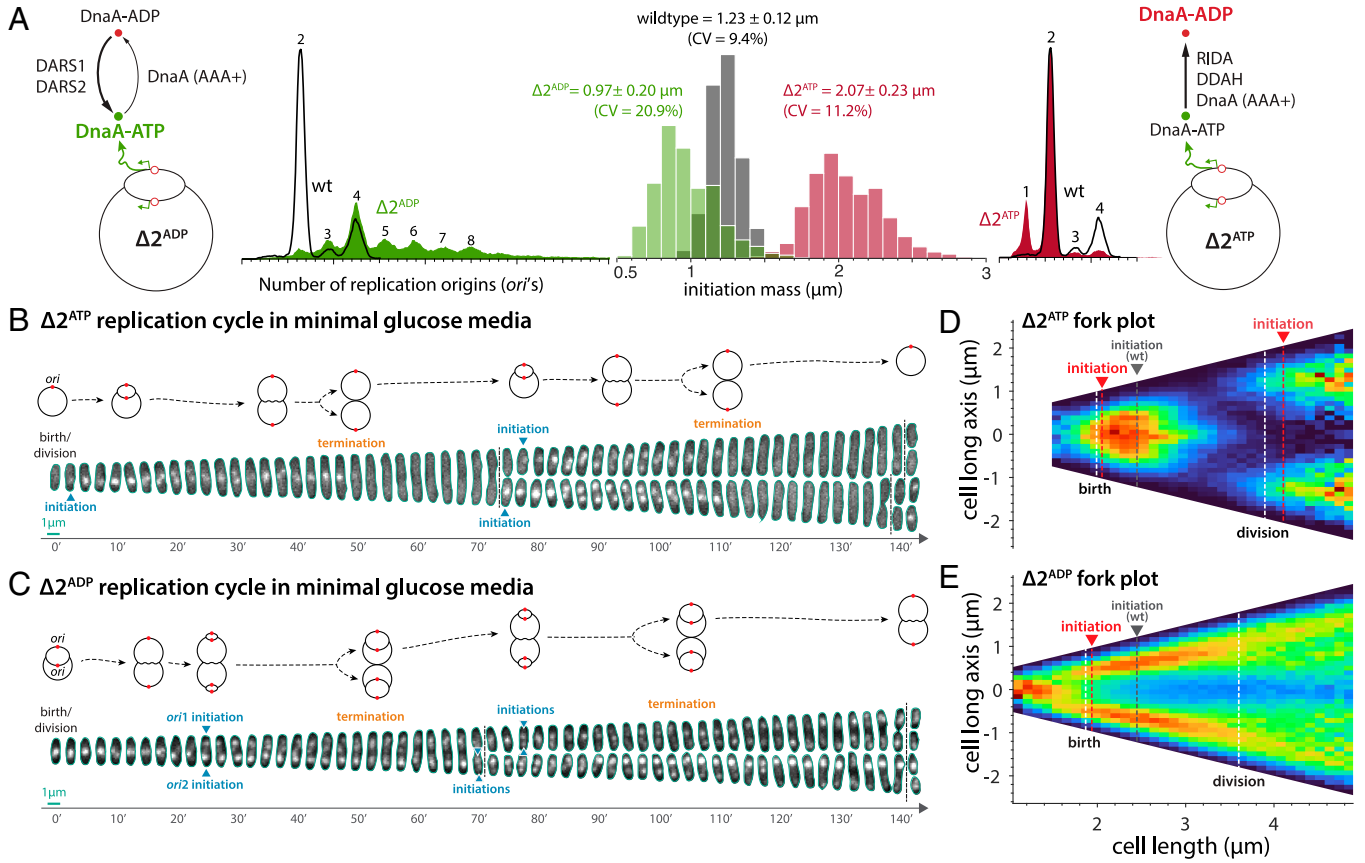

Fig. 2. Opposing effects of the $\Delta 2^{ATP}$ and $\Delta 2^{ADP}$ mutants on initiation. (*A*) The initiation mass distributions from mother-machine experiments and the flow-cytometry data. (*B* and *C*) Timelapse fluorescence imaging of $\Delta 2^{ATP}$ ($\Delta 2^{ADP}$) cells with chromosome configurations above. (*D* and *E*) The fork plot of the $\Delta 2^{ATP}$ ($\Delta 2^{ADP}$) cells shows the distribution of foci along the cell long axis in cells binned by cell length. The dashed mean initiation lines are from the initiation mass distributions from (*A*).

initiation delay. The initiation mass distribution is shifted to the right, with an approximately 70% larger average and a slightly increased CV than the wild-type (Fig. 2*A*). Flow-cytometry data indicate that most cells contain either one or two replication origins (*oriC*'s) (Fig. 2*A* and *SI Appendix*, Fig. S6), suggesting nonoverlapping cell cycles. In other words, initiation typically occurs after cell birth, a trend supported by the fork plot in Fig. 2*D* (*Materials and Methods*) and illustrated in a real example in Fig. 2*B*. Noticeably, the replisome foci distribution in the cell is highly symmetric in this mutant, which differs from the discovery in a previous study of a mutant with a similar genotype (4).

By contrast, $\Delta 2^{ADP}$ initiates prematurely, as evidenced by the smaller initiation mass than the wild-type cells (Fig. 2*A*). The average initiation mass is smaller by around 20%, while the CV increases significantly from 10% to above 20% (Fig. 2*A*). This mutant was particularly difficult to analyze due to its highly noisy initiation behavior. For example, unlike the wild-type cells in the same growth condition, $\Delta 2^{ADP}$ cells typically undergo overlapping cell cycles with a new round of replication initiates before the previous round of replication terminates (Fig. 2*C*), a challenging condition for tracking replication cycles using image analysis (*Materials and Methods*). Based on the fork plot in Fig. 2*E*, we suspect that the actual mean initiation mass could be even smaller and the CV larger than our statistics suggest (see *SI Appendix*, Fig. S5 for estimation details).

These results indicate that the DnaA-ATP → DnaA-ADP and DnaA-ADP → DnaA-ATP conversion elements have opposing effects on initiation.

Δ4 *E. coli* Exhibits a Near Wild-Type Phenotype Despite the Absence of All Known Extrinsic DnaA-ATP ↔ DnaA-ADP Conversion Elements. As the $\Delta 2^{ATP}$ (ΔDARS1 ΔDARS2) and $\Delta 2^{ADP}$ (Δ*hda* Δ*datA*) show the opposing effects, we wondered whether we could delete all four extrinsic conversion elements (DARS1, DARS2, *hda*, and *datA*) (Fig. 3*A*). To the best of our knowledge, such attempts had never been made before, probably because of the apparent importance of DnaA-ADP ↔ DnaA-ATP in initiation control. Indeed, deletion of each of these elements typically impacts the cells adversely, as seen in Fig. 2 and *SI Appendix*, Fig. S4 (25, 30, 43).

To our surprise, however, the Δ4 (ΔDARS1 ΔDARS2 Δ*hda* Δ*datA*) *E. coli* not only was viable but also exhibited a near wild-type initiation phenotype. Specifically, the average initiation mass remained close to the wild-type cells, with a modest increase in the CV of the initiation mass from 9.4% to 16.0% (Fig. 3*A*). This is consistent with the flow-cytometry data, which shows a small increase in average number of origins per cell with slight initiation asynchrony (revealed by the peaks corresponding to 3, 5, and 6 replication origins, in addition to 2 and 4 expected for two overlapping cell cycles) (Fig. 3*A* and *SI Appendix*, Fig. S6). The statistics and flow-cytometry data are also consistent with the fork plots (Fig. 3 *C* and *D*), where Δ4 and wild-type cells show similar fork patterns but Δ4 is noisier. Further, the Δ4 and wild-type cells have similar average values in other parameters, including the growth rate and cell sizes, although the CV is generally larger in Δ4 (*SI Appendix*, Fig. S1).

These results suggest that the rate of DnaA-ADP → DnaA-ATP by DARS1 + DARS2 and DnaA-ATP → DnaA-ADP

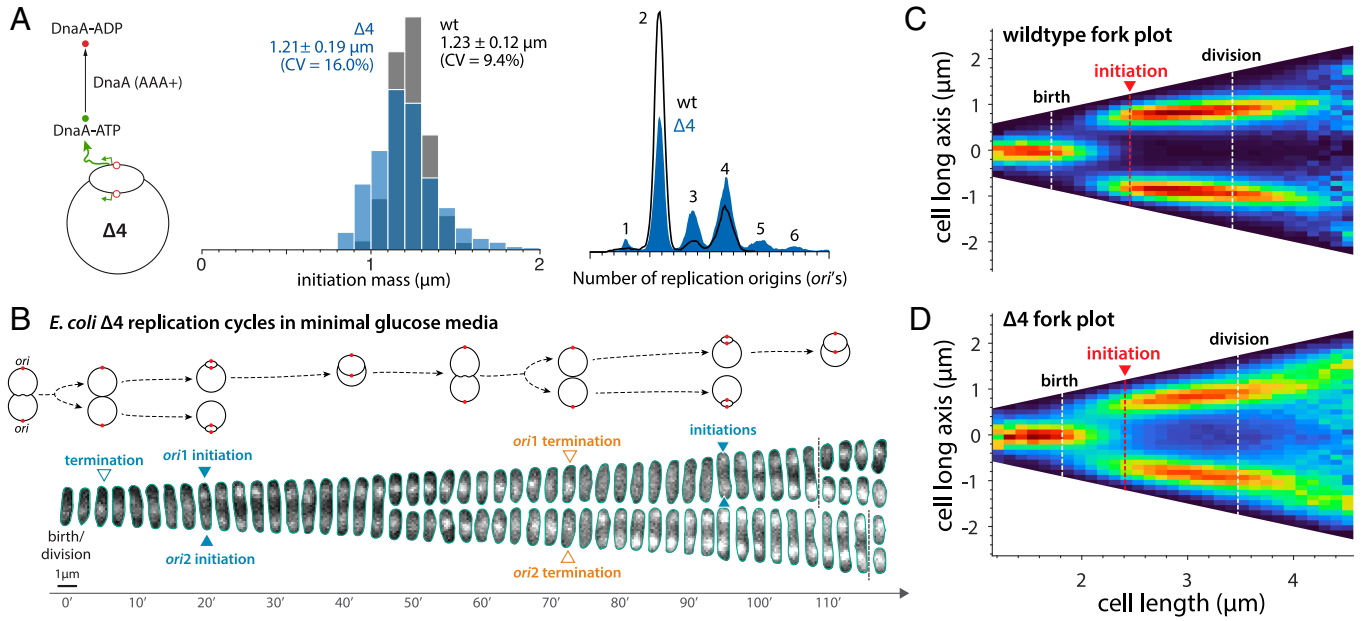

Fig. 3. Robustness of Δ4 *E. coli*. (*A*) The initiation mass distributions and the flow-cytometry data for Δ4 cells vs. wild-type cells. (*B*) Timelapse fluorescence imaging of 4 cells with chromosome configurations shown above. (*C* and *D*) fork plots for wild-type cells vs. Δ4 cells.

by *hda* + *datA* (RIDA and DDAH) largely compensate each other in the wild-type cells. In the Δ4 cells, their opposing effects should largely cancel out, only mildly compromising the initiation processes.

The Intrinsic ATPase Activity of DnaA Can be Sufficient for the Initiation Control. The unexpectedly robust initiation control in the Δ4 *E. coli* raises the fundamental question: if only DnaA-ATP is required for initiation at *oriC*, why does *E. coli* maintain both forms of DnaA and the intricate DnaA-ATP ↔ DnaA-ADP conversion elements? We present two orthogonal experimental results that show both forms of DnaA are required to improve initiation stability to a wider range of physiological conditions.

First, we gradually overproduced wild-type DnaA ($DnaA^{WT}$) in the Δ4 background in intermediate growth conditions (Fig. 4*A*). The Δ4 cells were viable up to 1.7-fold the wild-type level of DnaA and showed reinitiation beyond that point. By contrast, wild-type cells tolerated a significantly higher level of DnaA and only overinitiated modestly (Fig. 4*A*). Nevertheless, that the Δ4 *E. coli* was viable at the elevated level of DnaA suggests a significant ATPase activity of DnaA in vivo.

Next, we also investigated Δ4 *E. coli*'s tolerance of two different DnaA mutants. $DnaA^{R334A}$ is known for a significantly decreased ATPase activity (thus a higher DnaA-ATP level) (39, 44), whereas $DnaA^{T174P}$ shows an increased activity (thus a lower DnaA-ATP level) (45). The Δ4 cells did not tolerate additional $DnaA^{R334A}$ at all, likely due to the elevated DnaA-ATP level, compared to the wild-type cells (*SI Appendix*, Fig. S2*A*). Flow-cytometry data indicated overinitiation with a varying degree in both Δ4 and wild-type cells with $DnaA^{R334A}$ (*SI Appendix*, Fig. S2*A*).

On the other hand, the fast ATPase $DnaA^{T174P}$ variant did not cause a significant change in the average initiation mass at low to intermediate overproduction for both Δ4 and wild-type cells. Upon strong overproduction of $DnaA^{T174P}$, initiation was delayed (*SI Appendix*, Fig. S2*B*). We interpret these results as DnaA-ATP → DnaA-ADP in Δ4 was already sufficient for stable initiation, until high levels of DnaA-ADP by $DnaA^{T174P}$ became detrimental to the initiation process. One possible mechanistic cause is the formation of short DnaA-ADP oligomers following the de novo synthesis of $DnaA^{T174P}$, making DnaA-ATP unable to compete for initiation in this strain (46).

These results underscore that the intrinsic ATPase activity is sufficient for the observed wild-type phenotype of Δ4 in intermediate growth conditions, but their ability to buffer the impact of DnaA-ATP or DnaA-ADP level perturbations is less than the wild-type cells.

Extrinsic DnaA-ATP ↔ DnaA-ADP Conversion Elements Improve Initiation Stability to Multifork Replication. To assess the robustness of Δ4 cells to physiological perturbations, we tracked the replication cell cycle in various growth conditions. Under slow growth conditions, Δ4 cells exhibit near wild-type growth with slightly noisier replication initiation (a larger CV) compared to wild-type cells (Fig. 4*B* and *SI Appendix*, Fig. S4). However, their differences become significant under fast growth conditions, with the Δ4 *E. coli* showing more asynchronous initiations (Fig. 4*B*), resulting in growth defects (*SI Appendix*, Figs. S4 and S5). These results suggest that Δ4 cells are less robust against perturbations in fast growth conditions compared to wild-type cells.

Previously, we predicted using our initiator-titration model v2 that *E. coli* cells lacking external DnaA-ATP ↔ DnaA-ADP conversion elements can develop initiation instability during multifork replication (33). In this model, the initiation mass can oscillate between two values as the mass-doubling time becomes shorter than the C period ($C/\tau > 1$) (Fig. 4*C*). This unstable initiation can span a significant range of physiological conditions, shown as the shaded island in the C/τ vs. initiation mass in Fig. 4*C*. When two consecutive initiation events are close enough to be in the same generation, reinitiation occurs.

In the glucose minimal medium, C/τ was 0.84 ± 0.25 for Δ4 *E. coli* (Fig. 4*C*). Therefore, a subpopulation of Δ4 cells can enter the multifork replication regime ($C/\tau > 1$) due to the large variation of the doubling time and C period. Indeed, such predicted oscillations can be seen in our single-cell tracking experiment with *E. coli* Δ4 (Fig. 4*D*).

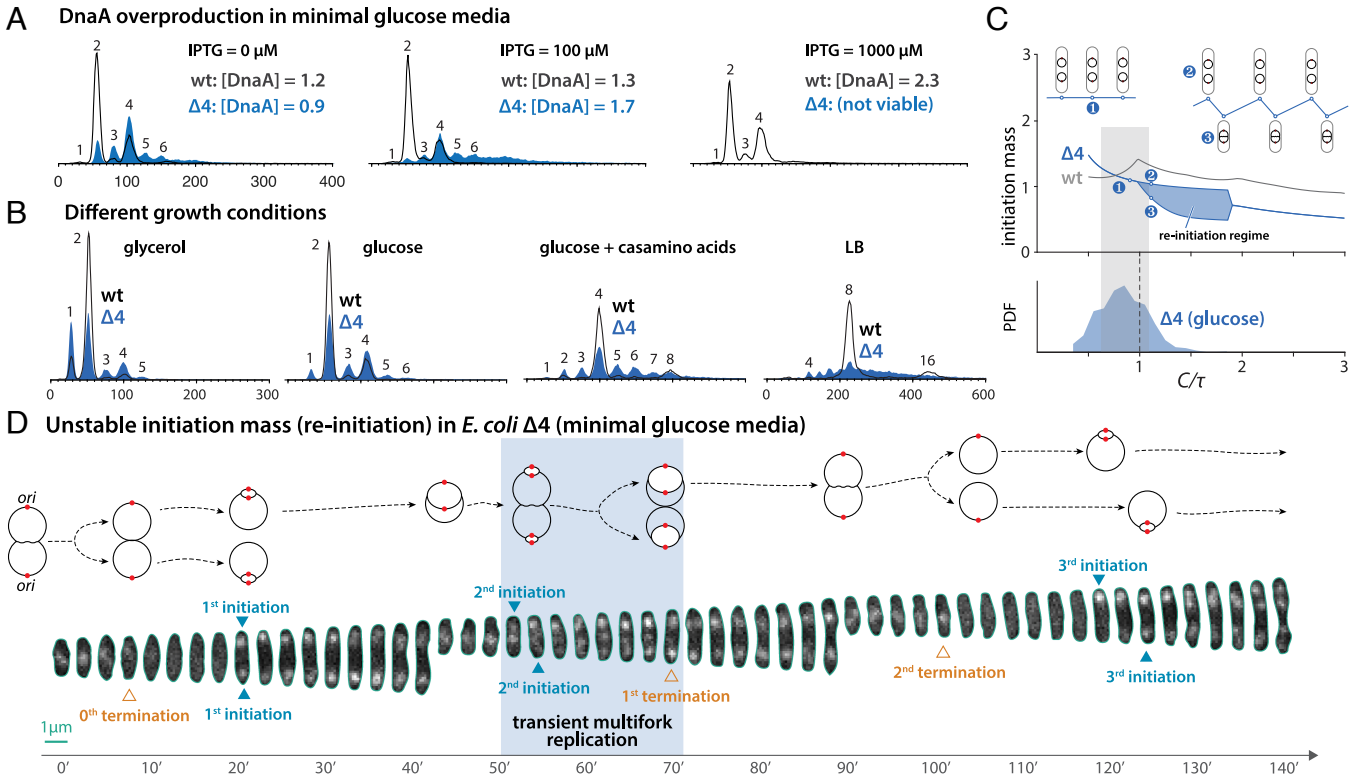

Fig. 4. Δ4 cells vs. wild-type cells in perturbations of DnaA concentration and growth conditions. (*A*) Flow-cytometry data of wild-type and Δ4 cells under different induction levels of an extra copy of *dnaA* gene on a plasmid. (*B*) Flow-cytometry data of wild-type and Δ4 cells under different growth conditions. (*C*) Theoretical predictions from the initiator-titration model v2 (33). *Lower* panel: The distribution of C/τ for Δ4 cells in the glucose condition. (*D*) A time-lapse imaging of Δ4 cells in the glucose condition as an example of unstable initiation mass. The chromosome configurations over time are illustrated above.

In rich media (MOPS rich glycerol), we measured the average $C/\tau \approx 1.2-1.3$ by mother machine (*SI Appendix*, Fig. S5), indicating that most Δ4 cells are in the reinitiation regime (Fig. 4*C*). We were unable to track the replication cycles at the single-cell level due to significant reinitiations and asynchrony. Nevertheless, the noisy initiation in Δ4 *E. coli* observed in both flow-cytometry (peaks at the odd numbers) and mother-machine experiments is well aligned with the predicted initiation instability.

The initiation instability of Δ4 *E. coli* during multifork replication can be understood intuitively. Δ4 *E. coli* lacks, among others, DnaA-ATP → DnaA-ADP conversion at the replication fork by RIDA. Therefore, Δ4 *E. coli* has a higher level of DnaA-ATP compared to wild-type *E. coli*, making Δ4 *E. coli* cells prone to reinitiation (see the next section and Fig. 5). Based on these results, we suggest that the role of extrinsic DnaA-ATP ↔ DnaA-ADP conversion elements is to extend initiation stability to multifork replication.

DnaA-ATP/DnaA-ADP Ratio and *dnaA* Promoter Activity in Wild-Type, Δ2, and Δ4 *E. coli*. In wild-type *E. coli* cells, the DnaA-ATP/DnaA-ADP is approximately 0.3 (25–27). In $\Delta 2^{ATP}$, DnaA-ATP/DnaA-ADP should be significantly lower because the triple-deletion *E. coli* strain (Δ*hda* ΔDARS1 ΔDARS2) shows a nearly 40% reduction in the DnaA-ATP/DnaA-ADP compared to the single deletion of Δ*hda* (26). By contrast, the $\Delta 2^{ADP}$ cells exhibit a higher level of DnaA-ATP and DnaA-ATP/DnaA-ADP ≃ 0.9 (27). In *E. coli* Δ4, we expect a higher level of DnaA-ATP and DnaA-ATP/DnaA-ADP compared to the wild-type cells since *E. coli* Δ4 shows the overinitiation phenotype (flow-cytometry data in Figs. 4 and 5).

To experimentally test our predictions on the DnaA-ATP/DnaA-ADP level in the Δ2 and Δ4 *E. coli*, we used *dnaAp* fused to *lacZ* encoded in the plasmid pTACDNAA that we developed previously (47). The rationale is that *dnaAp* autorepression is more efficient at a higher DnaA-ATP level (and thus at higher DnaA-ATP/DnaA-ADP for fixed [DnaA]; Fig. 5*C*) (10, 13). Our experimental results in Fig. 5*A* (*Left*) agree with our predictions.

We also tested our predictions using an independent method. Since the level of DnaA is proportional to the *dnaA* gene dosage and the promoter strength, we can predict the promoter strength by directly measuring the *ori* copy number (Fig. 5*B*) and DnaA level (Fig. 5 *C* and *D*), assuming that DnaA stability is not affected by ATP/ADP binding (48). Fig. 5*A* (*Right*) is the prediction based on our mathematical model (*SI Appendix*, section A) and data in Fig. 5 *B* and *D*.

Notice that the DnaA levels (Fig. 5*D*) and the GFP *dnaA* transcriptional reporter levels (Fig. 5*E*) are similar between wild-type and Δ4 *E. coli*. This is the consequence of the reduced *dnaAp* activity (Fig. 5*A*) and the increased gene dosage (Fig. 5*B*) compensating with each other in Δ4. More specifically, the predicted increase of DnaA-ATP/DnaA-ADP ratio in Δ4 is consistent with the slight overinitiation shown in Fig. 3*A*. This is also in agreement with the previously reported (Δ*hda* ΔDARS1 ΔDARS2) triple mutant (equivalent of our $\Delta 2^{ATP}$ cells deficient in Hda) having an increased DnaA-ATP/DnaA-ADP of 0.4 relative to the wild-type level of 0.3 (26). A further removal of *datA* is expected to slightly increase the ratio by ∼15% according to previous studies (27, 49).

In the next section, we explain how these results lead to the different initiation potential in the Δ2 and Δ4 cells.

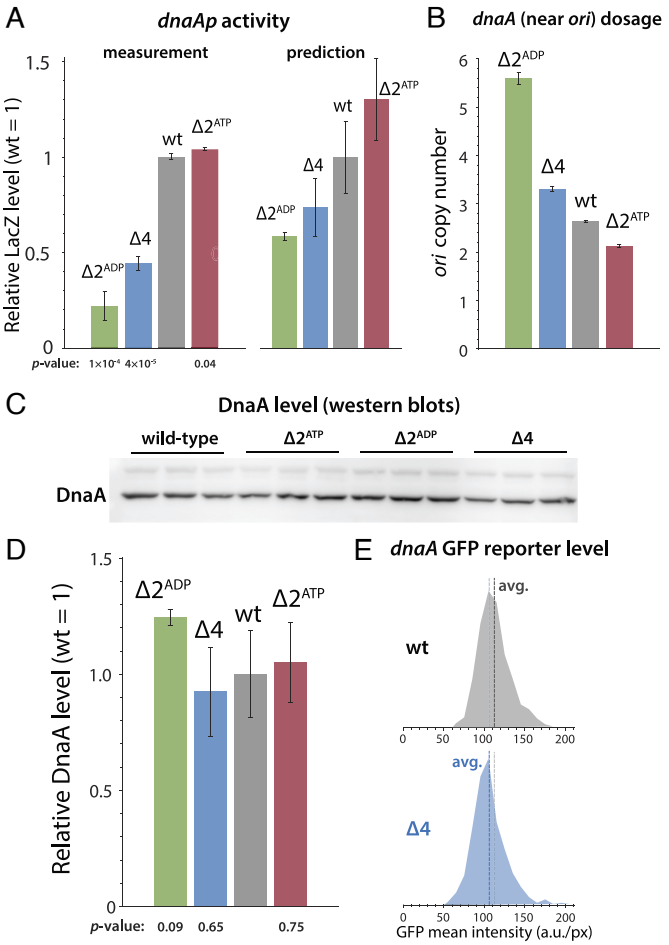

Fig. 5. The *dnaA* promoter (*dnaA*) activity is a good proxy of the relative DnaA-ATP/DnaA-ADP ratio. (*A*) *Left* panel: *dnaAp* activity measured by β-galactosidase assay using pTACDNAA plasmids encoding a copy of *dnaAp::lacZ* (47). The *P*-value between the wild-type and each Δ mutant is calculated by a two-sample *T* test. *Right* panel: *lacZ* expression level predicted using a mathematical model (*SI Appendix*, section A) and data in (*B*) and (*D*). (*B*) *dnaA* gene dosage is approximated by the average *ori* copy number per cell measured by flow cytometry. (*C* and *D*) Average DnaA concentration in wild-type, Δ2 and Δ4 mutants by western blots. Note that each strain is represented by three biological replicates. (*E*) *dnaA* transcription level is measured by a GFPmut2 transcription reporter in wild-type and Δ4 cells, consistent with the western blots in (*C*). See more details in Fig. 6. All error bars are SE of the replicates.

The Initiator-Titration Model v2 Can Explain the Δ2 and Δ4 Behaviors. Recently, we extended the initiator-titration model originally proposed by Hansen et al. (33, 36). In this initiator-titration model v2, we took into account the conversion of DnaA-ATP and DnaA-ADP. The key idea underlying both versions of the model is that DnaA (either form) proteins are first titrated by the DnaA boxes distributed along the chromosome before initiation, dividing the replication cycle into two sequential stages, namely, titration followed by initiation (Fig. 6*A*).

During the titration stage, the initiation "potential" is strongly suppressed as DnaA proteins (be they DnaA-ATP or DnaA-ADP) are titrated by the large number of high-affinity chromosomal DnaA boxes (10, 50, 51). As most of the chromosomal DnaA boxes become occupied, DnaA-ATP molecules will start to cooperatively bind to the cluster of low-affinity DnaA boxes at the origin of replication (*oriC*), thereby increasing the initiation potential (9, 14, 15). Meanwhile, DnaA-ADP can only bind to the chromosomal DnaA boxes but not at the low-affinity DnaA boxes within *oriC*, sharpening the initiation potential at *oriC* (33). Upon initiation, the number of DnaA boxes at *oriC* doubles, and *oriC* is sequestered by SeqA (52). The initiation potential thus drops significantly upon initiation and remains low during DNA replication due to the increased RIDA and DDAH activities.

By translating the initiator-titration model v2 to initiation potential, we can understand the behavior of $\Delta 2^{ATP}$, $\Delta 2^{ADP}$, and Δ4 in the following manner (Fig. 6*B*).

1. $\Delta 2^{ATP}$: the level of DnaA-ATP is lower than the wild-type, thus initiation delays since binding of the lowered level of DnaA-ATP to *oriC* is slowed down. DnaA titration and the related initiation potential are largely unaffected since both DnaA-ATP and DnaA-ADP can bind the high-affinity chromosomal DnaA boxes.
2. $\Delta 2^{ADP}$: The overall potential is markedly elevated due to the significantly higher level of DnaA-ATP, and it remains high after initiation due to the absence of RIDA and DDAH, both of which provide negative feedback on initiation (33). This can cause reinitiations.
3. Δ4: The overall initiation potential is still elevated due to the lack of RIDA and DDAH. Δ4 *E. coli* also lacks DARS1/2 and thus has a reduced DnaA-ADP → DnaA-ATP activity, alleviating the effect of missing RIDA and DDAH. However, due to the generally elevated level of DnaA-ATP, a modest additional increase in DnaA-ATP can cause reinitiation in the Δ4 cells, as seen in the $DnaA^{R334A}$ mutant experiment discussed earlier (*SI Appendix*, Fig. S2*A*).

Both Wild-type and Δ4 *E. coli* Show Nearly Constant Concentrations of DnaA During Cell Elongation. One of the major assumptions of the initiator-titration model v2 is the balanced biosynthesis of DnaA. In the practical aspect, balanced biosynthesis leads to constant protein concentration during cell elongation (1). This is in stark contrast to eukaryotic cell cycle controls dominated by programmed gene expression and protein degradation, causing changes in protein concentrations, such as oscillations for cyclins.

We tracked the DnaA level using a fast-maturing GFP in the mother machine (53). We found that the single-cell *dnaA* transcription levels were indeed practically constant during steady-state cell elongation despite large fluctuations (Fig. 6 *C*, solid lines). However, when we aligned the time series by the initiation events, we noticed a slight decrease of the GFP concentration at initiation in both wild-type cells and Δ4 cells. The decrease in the GFP concentration is due to the plateau of the total GFP starting at initiation (Fig. 6*C*, *Inset*), likely due to temporary repression of *dnaA* transcription by SeqA sequestration (52, 54–56) and *dnaA* autoregulation (57, 58). The mild decrease in *dnaA* promoter activity post initiations is also consistent with a recent study (59).

Nevertheless, as seen in the mean GFP level vs. time, the impact of *dnaA* repression is modest compared to the scale of protein concentration fluctuations (Fig. 6*C*). Therefore, the weak oscillation of the DnaA concentration unlikely can explain the precise initiation control (CV ≤ 10%). We thus conclude that DnaA production is nearly balanced, well aligned with the initiator-titration models (33, 36) and the adder principle of size control (1, 60, 61).

The constancy of DnaA level in Δ4 *E. coli* has important implications. To see this, consider the balanced biosynthesis of DnaA, $\frac{dN_{ATP}}{dt} = \lambda N_{tot} - \nu N_{ATP}$, $\frac{dN_{tot}}{dt} = \lambda N_{tot}$, and $\frac{dV}{dt} =$

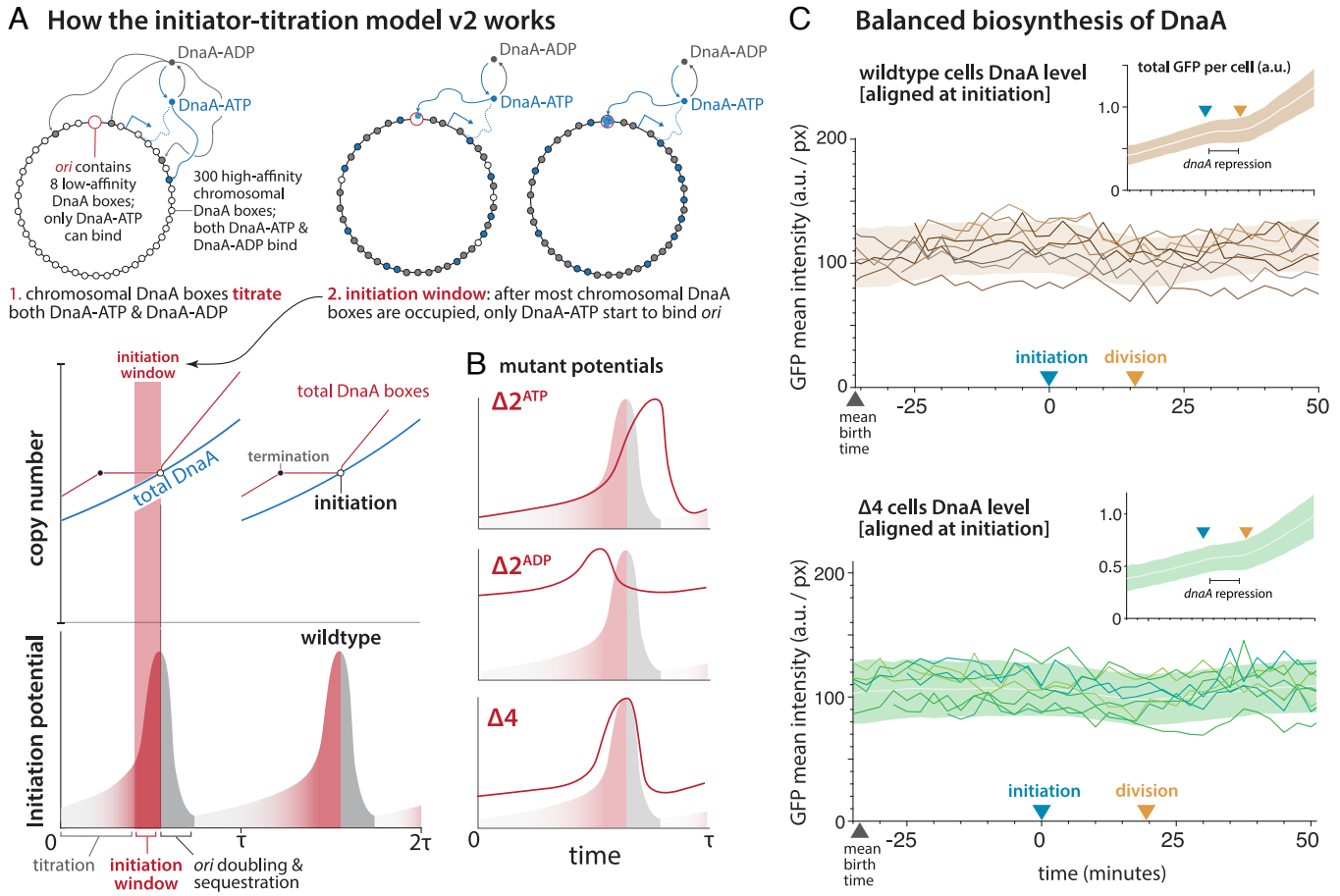

Fig. 6. The initiator-titration model v2 and the Δ2/Δ4 mutant behaviors. (*A*) The initiator-titration model v2 and the initiation potential for wild-type cells. (*B*) Illustration of the initiation potentials of $\Delta 2^{ATP}$, $\Delta 2^{ADP}$, and Δ4 compared with the wild-type. (*C*) The time-dependent transcription level of *dnaA* is measured by the GFPmut2 transcriptional reporter. Single-cell mean GFP intensity (in absolute unit) time series (solid lines) are aligned at initiation events. The average GFP level is similar between the wild-type and Δ4 cells (also see Fig. 5*D*). Despite a mild decrease after initiation, the nearly constant mean intensity level (white lines) indicates that DnaA concentration remains almost constant in both wild-type and Δ4 *E. coli*. Therefore, [DnaA-ATP] and [DnaA-ADP] also must be constant in Δ4 *E. coli* during steady-state cell elongation. Inset: the total GFP level per cell shows the effect of *dnaA* repression after initiation.

λV, where N_{ATP} is the number of DnaA-ATP, N_{tot} the total number of DnaA, V the cell volume, and λ the growth rate. The steady-state solution of these equations leads to [DnaA] = constant (Fig. 6*C*), [DnaA-ATP] = constant, and [DnaA-ADP] = constant during cell elongation (*SI Appendix*, section B). Since the protein concentrations are constant, the cell must accumulate a threshold number of initiator proteins to trigger a cell cycle event, such as DnaA for replication initiation (1, 60) or FtsZ for cell division (1). These conclusions represent a fundamental difference from eukaryotic cell cycle control based on oscillations of cyclin concentrations via programmed gene expression and/or protein degradation (62).

Discussion

In this work, we have shown that Δ4 *E. coli*, devoid of all known extrinsic regulatory elements for DnaA-ATP ↔ DnaA-ADP conversion (DARS1, DARS2, *hda*, and *datA*), can exhibit near wild-type phenotype for initiation control. An emerging picture from this study and our previous works (1, 33) is that the bacterial cell cycle control must depend on the protein counting mechanisms, rather than protein concentration sensing in eukaryotes. Since balanced biosynthesis is the hallmark of bacterial physiology (35), the differences between bacteria and eukaryotes are profound and merit further investigations in the future.

Apart from initiation, our Δ2 and Δ4 mutants show interesting features that warrant future investigation. For example, while Δ4 and $\Delta 2^{ADP}$ cells show colocalized replisomes (Figs. 1*C*, 2*C*, and 3*B*) consistent with recent reports (63–65), $\Delta 2^{ATP}$ cells show significantly different behaviors with one replisome focus splitting into two foci during DNA replication (Fig. 2*B*). It remains to be seen whether these differences reflect distinct overall chromosome organization as suggested previously (65) or more active interactions between replication forks.

Furthermore, more insightful information may be within reach based on new high-throughput data and mathematical modeling (61, 66–68), which can reveal the relationship between initiation and replication dynamics.

Finally, the conditionally robust initiation of the Δ4 cells and its mechanistic implications was a major surprise for us. At the same time, we also find them gratifying from an evolutionary perspective (69, 70). For example, the First Cell would only need one master regulator protein with intrinsic ATPase activity, and different organisms may have acquired organism-specific additional control mechanisms to extend the physiological space for robust initiation control and stability during evolution (Fig. 4). While modest in the cell-cycle timescale, their impact on the evolutionary timescale is unquestionable.

Materials and Methods

Growth Conditions. In flow-cytometry experiments and most of the mother-machine experiments, cells were grown in Lysogeny Broth (LB) or AB minimal medium (71) supplemented with 10 μg/mL thiamine and 0.2% glucose (ABT-glucose), 0.2% glucose + 0.5% casamino acids (ABT-glucose + casamino acids), or 0.2% glycerol (ABT-glycerol). Only in the mother-machine experiments in fast growth conditions (*SI Appendix*, Fig. S5), we used MOPS rich media (5, 72) supplemented with 0.2% glycerol. When necessary, antibiotics were added in the following concentrations: kanamycin, 50 μg/mL; chloramphenicol, 20 μg/mL; ampicillin, 150 μg/mL.

Construction of Mutants of DnaA-ATP ↔ DnaA-ADP Regulatory Elements. All strains used were derivatives of *E. coli* K-12 MG1655 (F- λ- rph-1) (73). All deletions were performed by P1-mediated transduction (74). The Δ*hda* Δ*datA* strain was constructed by transducing Δ*hda* into a Δ*datA* strain and plating it on an ABT-glycerol medium as described previously (43, 75). The individual ΔDARS1:*cat* (ALO4313) and ΔDARS2:*cat* (ALO4254) mutants were constructed previously (28, 76) using the λ-red procedure (77). Before combining the ΔDARS1 and ΔDARS2, the *cat* resistance marker was cured from ALO4313 using pCP20 (78). The Δ4 strain (ΔDARS1 ΔDARS2 Δ*hda* and Δ*datA*) was constructed by combining the above by P1 transduction. All strains were whole-genome sequenced to confirm the presence of the mutations and to ensure that no suppressors appeared (*SI Appendix*, Table S2).

Construction of Fluorescence-Labeled Strains. To track the initiation of chromosome replication in the strains, we inserted a fluorescence-labeled sliding-clamp of the replisome, *dnaN-yPet* (1, 79), into the wild-type, $\Delta 2^{ATP}$, $\Delta 2^{ADP}$, and Δ4 strains through P1 transduction (*SI Appendix*, Table S1).

To measure the DnaA level while tracking initiations in the wild-type and Δ4, we inserted a fast-maturing GFP, *gfpmut*2 (80), between the endogenous *dnaA* and *dnaN* as a transcription reporter for *dnaA*. Due to the similarity of the excitation spectra between YPet and GFPmut2, we used mCherry instead of YPet as a fluorescent tag for the replisome. The *gfpmut*2 and the *mcherry* genes were assembled with an ampicillin resistance gene using Gibson assembly, and the entire fragment was inserted to the *dnaA* operon on the chromosome of both the wild-type and Δ4 through recombineering (81). For Δ4, we verified the loci of previous deletions through sequencing after recombineering.

Plasmids. Overexpression of DnaA was performed using pLR40 (82).

The pLRR334A with $DnaA^{R334A}$ was created using the primers: CTG CAG GTC GAC GGA TCC CCA A, AGC CCA GCG CGT CGG CCG CCA T, TCGCCAAGCGTCT-ACGATCTAACGTAGCTGAGCTGGAAGGGGCGCTGAAC, and GTTCAGCGCCCCTTCCA-GCTCAGCTACGTTAGATCGTAGACGCTTGGCGA.

The pLRT174P with $DnaA^{T174P}$ was created using primers: CTG CAG GTC GAC GGA TCC CCA A, AGC CCA GCG CGT CGG CCG CCA T, ATGGCGGCC-CGGGTCTGGGTAAAACTCACC, and ACCCAGACCCGGGCCGCCATAAAGGAACAA.

DnaA Level Measurements. Samples for western blots were prepared as described previously (48). Quantification of protein levels and analysis were performed using ImageJ software and the signal relative to the wildtype was calculated.

Flow Cytometry. Cells were balanced in exponential growth for more than 10 generations and incubated with 300 μg/mL rifampicin and 36 μg/mL at 37 °C for 4 h, allowing ongoing replication cycles to terminate. Cells were harvested and resuspended in 100 μL 10 mM Tris-HCl, pH 7.4, and fixed by adding 1 mL of 77% ethanol and stored at 4 °C.

Before flow cytometric analysis, fixed cells were pelleted by centrifugation at 15,000 rcf for 15 min. The supernatant was discarded, and the pellet was resuspended in 150 μL staining solution (90 μg/mL mithramycin, 20 μg/mL ethidium bromide, 10 mM $MgCl_2$, 10 mM Tris-HCl, pH 7.4). Samples were kept on ice for a minimum of 10 min before analysis.

We performed flow-cytometry experiments as described previously (83) using an Apogee A10 system. A minimum of 30,000 cells for each sample were analyzed.

Growth Rates Quantifications. Overnight cell cultures were back diluted by >4,000 folds and then incubated in flasks in 37 °C water incubator. The OD_{600} of cell cultures was measured using a spectrophotometer (Thermo Scientific GENESYS 20). The data points when cells entered exponential growth (OD_{600} between 0.01 and 0.2) were taken into account for determining doubling times. Doubling times were determined by linear regression of $\log_2(OD_{600})$ versus time.

β-Galactosidase Assay. Cells transformed with pTACDNAA (47) were grown in ABT-glucose (0.2%) in presence of carbenicillin (100 μg/mL) and permeabilized with toluene. The β-galactosidase activity was determined as previously described (74).

Microfluidic Experiments. We used PDMS-based mother machines to track single-cell lineages (1, 53, 84). To guarantee the same experimental conditions for control experiments, we designed duplex mother machines and multiplex mother machines that contain two main trenches and sixteen main trenches on each device, respectively (*SI Appendix*, Fig. S7). Each side of the main trench consists of 2,000 channels with a width ranging from 1.1 to 1.5 μm in design. The inlet of each main trench was connected to a syringe with a growth medium by Teflon tubing. The syringes were controlled by syringe pumps (PHD Ultra, Harvard Apparatus, MA) to maintain a constant flow rate of 1 mL/hour in each main trench.

In preparation of a mother-machine experiment, a single colony was inoculated in 1 mL ABT-glucose, containing appropriate antibiotics, and incubated overnight at 37 °C in a water-bath shaker. Cells were then diluted 1,000-fold into fresh media and balanced in an exponential phase for more than 10 generations. When reaching an OD_{600} of 0.1 to 0.15, cells were pelleted, concentrated, and injected into the mother machine device prewashed with BSA to reduce cell adhesion in the device channels. A constant flow of fresh growth media was supplied through the device for the duration of the experiment, as described previously (1, 84). After setting up the microfluidics and the microscopy program, we waited around 3 h before imaging to ensure cells were in the steady state.

Microscopy. We performed phase contrast and fluorescence imaging tandemly on an inverted microscope (Nikon Ti-E) with Perfect Focus 3 (PFS3), 100× oil immersion objective (PH3, numerical aperture = 1.45), Obis lasers 488 nm (Coherent Inc., CA) as fluorescence light source, Chroma EYFP filter (49003-ET-EYFP), and Prime 95B sCMOS camera (Photometrics) (1). For data in Fig. 6*C*, we used Obis lasers in both 488 and 561 nm as well as a GFP/mCherry dual-band filter (59022-ET-EGFP/mCherry). The laser power for 488 nm excitation was 30 mW, and the exposure time was 100 ms. The laser power for 561 nm excitation was 40 mW, and the exposure time was 100 ms. The imaging time interval was 2.5 min for all the mother-machine experiments.

Image Analysis. We used our Napari-mm3 platform (85), following the developed protocol of mother-machine image analysis (85). Details of different parts of data analysis are as follows.

Cell segmentation. For cell segmentation, we used a machine-learning-based method, U-net, rather than the traditional Otsu method to obtain more reliable results (86).

Fluorescence kymographs. The cell segmentation results were also used in plotting time-lapse fluorescence images (kymographs), such as in Fig. 1*C*. In Adobe Illustrator (2023), a segmentation image and the corresponding fluorescence image were overlapped first, and the "image trace" function was applied to the segmentation image to track and smoothen the boundary of each segmented cell. We then used the function "make clipping mask" to obtain individual cell images with fluorescence inside.

Fork plots. For fork plots, we used a Laplacian of Gaussian method to identify fluorescence foci, as described previously (1). The position of foci along the cell's long axis (y axis) was recorded and binned by 1 pixel of the original image (0.11 μm). Cells were then binned by cell length (x axis) with 1 pixel (0.11 μm) in each bin. The number of foci in each pixel was counted for all daughter cells [mother cells not counted to avoid any aging effects (85)], and then normalized by the number of cells at the same cell length. Thus, the color in each pixel on

the fork plots shows the probability of foci appearing at that y-position in the cell in that cell length.

Initiation and termination identification. For single-cell initiation and termination data, we did manual annotation and inspection using two different methods. First, we used the results from foci identification as described previously in ref. 1. To ensure the first method was not biased by foci identification, our second method directly tracked foci from the subtracted fluorescence images on Napari (a new feature in Napari-mm3). We found that both methods produced similar distributions of the initiation mass for the wild-type, $\Delta 2^{ATP}$, and $\Delta 4$, while the foci in $\Delta 2^{ADP}$ was too messy to be tracked faithfully by the second method. We then adopted the foci tracking results from the first method as in Figs. 2 and 3. The cell length at initiations and terminations was recorded, and the initiation mass was defined as the cell length at initiation, divided by the number of origins [given the negligible change in cell width (84)].

Aligned fluorescence intensity time series. The mean intensity of a transcription reporter (such as GFPmut2) within a cell at each time point was calculated by averaging the intensity values (in absolute unit) along the mid-line of a cell using the function "morphology.medial_axis" in the Python package "skimage." The mean intensity time series for each cells were aligned by the initiation events (i.e., initiation time = 0). The average value was calculated at each time point (white line in Fig. 6*C*) and the standard value is shown by the shadow region. As for the total intensity shown in Fig. 6 *C*, *Insets*, it was calculated by integrating the intensity values of all pixels in a segmented cell.

Additional details of strain information and data analysis are described in *SI Appendix*.

Data, Materials, and Software Availability. The raw data for mother-machine experiments and flow-cytometry experiments have been uploaded on Dryad (87).

ACKNOWLEDGMENTS. We are deeply grateful to Tove Atlung, Tsutomu Katayama, and Shogo Ozaki for discussion and their invaluable advice, which led to Fig. 5. The work of H.F., C.J., M.S., and S.J. was supported by NIH Grant R35GM139622 and NSF Grant MCB-2016090 (to S.J.). The work of T.O.B., G.C., and A.L.-O. was supported through a Challenge program (NNF16OC0021700) from the Novo Nordisk Foundation, by Grant DNRF120 from the Danish National Research Foundation and by Grant 39854 from the Villum Foundation.

Author affiliations: [a]Department of Biology, University of Copenhagen, Copenhagen 2200, Denmark; and [b]Department of Physics, University of California San Diego, La Jolla, CA 92093

1. F. Si *et al*., Mechanistic origin of cell-size control and homeostasis in bacteria. *Curr. Biol.* **29**, 1760–1770.e7 (2019).
2. J. T. Sauls *et al*., Control of *Bacillus subtilis* replication initiation during physiological transitions and perturbations. *mBio* **10**, e02205-19 (2019).
3. M. Wallden, D. Fange, E. G. Lundius, Ö. Baltekin, J. Elf, The synchronization of replication and division cycles in individual *E. coli* cells. *Cell* **166**, 729–739 (2016).
4. A. Knöppel, O. Broström, K. Gras, J. Elf, D. Fange, Regulatory elements coordinating initiation of chromosome replication to the *Escherichia coli* cell cycle. *Proc. Natl. Acad. Sci. U.S.A.* **120**, e2213795120 (2023).
5. F. Si *et al*., Invariance of initiation mass and predictability of cell size in *Escherichia coli*. *Curr. Biol.* **27**, 1278–1287 (2017).
6. W. D. Donachie, Relationship between cell size and time of initiation of DNA replication. *Nature* **219**, 1077–1079 (1968).
7. S. Wold, K. Skarstad, H. B. Steen, T. Stokke, E. Boye, The initiation mass for DNA replication in *Escherichia coli* K-12 is dependent on growth rate. *EMBO J.* **13**, 2097–2102 (1994).
8. H. Zheng *et al*., General quantitative relations linking cell growth and the cell cycle in *Escherichia coli*. *Nat. Microbiol.* **5**, 995–1001 (2020).
9. T. Katayama, K. Kasho, H. Kawakami, The DnaA cycle in *Escherichia coli*: Activation, function and inactivation of the initiator protein. *Front. Microbiol.* **8**, 2496 (2017).
10. F. G. Hansen, T. Atlung, The DnaA tale. *Front. Microbiol.* **9**, 319 (2018).
11. K. Kasho, S. Ozaki, T. Katayama, IHF and Fis as *Escherichia coli* cell cycle regulators: Activation of the replication origin *oriC* and the regulatory cycle of the DnaA initiator. *Int. J. Mol. Sci.* **24**, 11572 (2023).
12. K. Sekimizu, D. Bramhill, A. Kornberg, ATP activates DnaA protein in initiating replication of plasmids bearing the origin of the *E. coli* chromosome. *Cell* **50**, 259–265 (1987).
13. C. Speck, C. Weigel, W. Messer, ATP- and ADP-DnaA protein, a molecular switch in gene regulation. *EMBO J.* **18**, 6169–6176 (1999).
14. K. C. McGarry, V. T. Ryan, J. E. Grimwade, A. C. Leonard, Two discriminatory binding sites in the *Escherichia coli* replication origin are required for DNA strand opening by initiator DnaA-ATP. *Proc. Natl. Acad. Sci. U.S.A.* **101**, 2811–2816 (2004).
15. S. Ozaki *et al*., A common mechanism for the ATP-DnaA-dependent formation of open complexes at the replication origin. *J. Biol. Chem.* **283**, 8351–8362 (2008).
16. C. E. Samitt, F. G. Hansen, J. F. Miller, M. Schaechter, In vivo studies of DnaA binding to the origin of replication of *Escherichia coli*. *EMBO J.* **8**, 989–993 (1989).
17. C. Nievera, J. J. C. Torgue, J. E. Grimwade, A. C. Leonard, SeqA blocking of DnaA–*oriC* interactions ensures staged assembly of the *E. coli* pre-RC. *Mol. Cell* **24**, 581–592 (2006).
18. M. Filutowicz, W. Ross, J. Wild, R. L. Gourse, Involvement of Fis protein in replication of the *Escherichia coli* chromosome. *J. Bacteriol.* **174**, 398–407 (1992).
19. V. T. Ryan, J. E. Grimwade, J. E. Camara, E. Crooke, A. C. Leonard, *Escherichia coli* prereplication complex assembly is regulated by dynamic interplay among Fis, IHF and DnaA. *Mol. Microbiol.* **51**, 1347–1359 (2004).
20. P. Polaczek, Bending of the origin of replication of *E. coli* by binding of IHF at a specific site. *New Biol.* **2**, 265–271 (1990).
21. M. Shimizu *et al*., Near-atomic structural model for bacterial DNA replication initiation complex and its functional insights. *Proc. Natl. Acad. Sci. U.S.A.* **113**, E8021–E8030 (2016).
22. J. P. Erzberger, M. L. Mott, J. M. Berger, Structural basis for ATP-dependent DnaA assembly and replication-origin remodeling. *Nat. Struct. Mol. Biol.* **13**, 676–683 (2006).
23. A. C. Leonard, J. E. Grimwade, Regulation of DnaA assembly and activity: Taking directions from the genome. *Annu. Rev. Microbiol.* **65**, 19–35 (2011).
24. L. Riber, J. Frimodt-Møller, G. Charbon, A. Løbner-Olesen, Multiple DNA binding proteins contribute to timing of chromosome replication in *E. coli*. *Front. Mol. Biosci.* **3**, 29 (2016).
25. J. Kato, T. Katayama, Hda, a novel DnaA-related protein, regulates the replication cycle in *Escherichia coli*. *EMBO J.* **20**, 4253–4262 (2001).
26. K. Fujimitsu, T. Senriuchi, T. Katayama, Specific genomic sequences of *E. coli* promote replicational initiation by directly reactivating ADP-DnaA. *Genes Dev.* **23**, 1221–1233 (2009).
27. K. Kasho, T. Katayama, DnaA binding locus datA promotes DnaA-ATP hydrolysis to enable cell cycle-coordinated replication initiation. *Proc. Natl. Acad. Sci. U.S.A.* **110**, 936–941 (2013).
28. J. Frimodt-Møller, G. Charbon, K. A. Krogfelt, A. Løbner-Olesen, DNA replication control is linked to genomic positioning of control regions in *Escherichia coli*. *PLoS Genet.* **12**, e1006286 (2016).
29. R. Kitagawa, T. Ozaki, S. Moriya, T. Ogawa, Negative control of replication initiation by a novel chromosomal locus exhibiting exceptional affinity for *Escherichia coli* DnaA protein. *Genes Dev.* **12**, 3032–3043 (1998).
30. G. Charbon, L. Bjørn, B. Mendoza-Chamizo, J. Frimodt-Møller, A. Løbner-Olesen, Oxidative DNA damage is instrumental in hyperreplication stress-induced inviability of *Escherichia coli*. *Nucleic Acids Res.* **42**, 13228–13241 (2014).
31. W. D. Donachie, G. W. Blakely, Coupling the initiation of chromosome replication to cell size in *Escherichia coli*. *Curr. Opin. Microbiol.* **6**, 146–150 (2003).
32. M. Berger, P. R. T. Wolde, Robust replication initiation from coupled homeostatic mechanisms. *Nat. Commun.* **13**, 6556 (2022).
33. H. Fu, F. Xiao, S. Jun, Bacterial replication initiation as precision control by protein counting. *PRX Life* **1**, 013011 (2023).
34. M. Schaechter, O. Maaloe, N. O. Kjeldgaard, Dependency on medium and temperature of cell size and chemical composition during balanced grown of *Salmonella typhimurium*. *J. Gen. Microbiol.* **19**, 592–606 (1958).
35. S. Jun, F. Si, R. Pugatch, M. Scott, Fundamental principles in bacterial physiology–history, recent progress, and the future with focus on cell size control: A review. *Rep. Prog. Phys.* **81**, 056601 (2018).
36. F. G. Hansen, B. B. Christensen, T. Atlung, The initiator titration model: Computer simulation of chromosome and minichromosome control. *Res. Microbiol.* **142**, 161–167 (1991).
37. K. Kasho, K. Fujimitsu, T. Matoba, T. Oshima, T. Katayama, Timely binding of IHF and Fis to DARS2 regulates ATP-DnaA production and replication initiation. *Nucleic Acids Res.* **42**, 13134–13149 (2014).
38. R. Sugiyama *et al*., A novel mode of DnaA–DnaA interaction promotes ADP dissociation for reactivation of replication initiation activity. *Nucleic Acids Res.* **47**, 11209–11224 (2019).
39. S. Nishida *et al*., A nucleotide switch in the *Escherichia coli* DnaA protein initiates chromosomal replication: Evidence from a mutant DnaA protein defective in regulatory ATP hydrolysis in vitro and in vivo. *J. Biol. Chem.* **277**, 14986–14995 (2002).
40. M. Su'etsugu, T. R. Shimuta, T. Ishida, H. Kawakami, T. Katayama, Protein associations in DnaA-ATP hydrolysis mediated by the Hda-replicase clamp complex. *J. Biol. Chem.* **280**, 6528–6536 (2005).
41. M. Su'etsugu, M. Takata, T. Kubota, Y. Matsuda, T. Katayama, Molecular mechanism of DNA replication-coupled inactivation of the initiator protein in *Escherichia coli*: Interaction of DnaA with the sliding clamp-loaded DNA and the sliding clamp-Hda complex. *Genes Cells* **9**, 509–522 (2004).
42. M. Su'etsugu *et al*., The DnaA n-terminal domain interacts with Hda to facilitate replicase clamp-mediated inactivation of DnaA. *Environ. Microbiol.* **15**, 3183–3195 (2013).
43. G. Charbon *et al*., Iron chelation increases the tolerance of *Escherichia coli* to hyper-replication stress. *Sci. Rep.* **8**, 1–14 (2018).
44. K. Nakamura, T. Katayama, Novel essential residues of Hda for interaction with DnaA in the regulatory inactivation of DnaA: Unique roles for Hda AAA box VI and VII motifs. *Mol. Microbiol.* **76**, 302–317 (2010).
45. S. Gon *et al*., A novel regulatory mechanism couples deoxyribonucleotide synthesis and DNA replication in *Escherichia coli*. *EMBO J.* **25**, 1137–1147 (2006).
46. H. Kawakami, K. Keyamura, T. Katayama, Formation of an ATP-DnaA-specific initiation complex requires DnaA arginine 285, a conserved motif in the AAA+ protein family. *J. Biol. Chem.* **280**, 27420–27430 (2005).
47. G. Charbon *et al*., Suppressors of DnaA(ATP) imposed overinitiation in *Escherichia coli*. *Mol. Microbiol.* **79**, 914–928 (2011).
48. G. Charbon *et al*., Energy starvation induces a cell cycle arrest in *Escherichia coli* by triggering degradation of the DnaA initiator protein. *Front. Mol. Biosci.* **8**, 629953 (2021).
49. T. Katayama, K. Fujimitsu, T. Ogawa, Multiple pathways regulating DnaA function in *Escherichia coli*: Distinct roles for DnaA titration by the data locus and the regulatory inactivation of DnaA. *Biochimie* **83**, 13–17 (2001).
50. S. Schaper, W. Messer, Interaction of the initiator protein DnaA of *Escherichia coli* with its DNA target. *J. Biol. Chem.* **270**, 17622–17626 (1995).

51. R. S. Fuller, B. E. Funnell, A. Kornberg, The dnaA Protein Complex with the *E. Coli* Chromosomal Replication Origin (*oriC*) and Other DNA Sites. *Cell* **38**, 889–900 (1984).
52. M. Lu, J. L. Campbell, E. Boye, N. Kleckner, SeqA: A negative modulator of replication initiation in *E. coli*. *Cell* **77**, 413–426 (1994).
53. P. Wang *et al*., Robust growth of *Escherichia coli*. *Curr. Biol.* **20**, 1099–1103 (2010).
54. J. L. Campbell, N. Kleckner, *E. coli oric* and the dnaA gene promoter are sequestered from dam methyltransferase following the passage of the chromosomal replication fork. *Cell* **62**, 967–979 (1990).
55. P. W. Theisen, J. E. Grimwade, A. C. Leonard, J. A. Bogan, C. E. Helmstetter, Correlation of gene transcription with the time of initiation of chromosome replication in *Escherichia coli*. *Mol. Microbiol.* **10**, 575–584 (1993).
56. A. Løbner-Olesen, M. G. Marinus, F. G. Hansen, Role of SeqA and dam in *Escherichia coli* gene expression: A global/microarray analysis. *Proc. Natl. Acad. Sci. U.S.A.* **100**, 4672–4677 (2003).
57. T. Atlung, E. S. Clausen, F. G. Hansen, Autoregulation of the dnaA gene of *Escherichia coli* K12. *Mol. Gen. Genet.* **200**, 442–450 (1985).
58. C. Saggioro, A. Olliver, B. Sclavi, Temperature-dependence of the DnaA–DNA interaction and its effect on the autoregulation of dnaA expression. *Biochem. J* **449**, 333–341 (2012).
59. I. Iuliani, G. Mbemba, M. C. Lagomarsino, B. Sclavi, Direct Single-Cell Observation of a Key Escherichia Coli Cell-Cycle Oscillator. *Sci. Adv.* **10** (2024), https://doi.org/10.1126/sciadv.ado5398.
60. L. Sompayrac, O. Maaløe, Autorepressor model for control of DNA replication. *Nat. New Biol.* **241**, 133–135 (1973).
61. G. Le Treut, F. Si, D. Li, S. Jun, Quantitative examination of five stochastic cell-cycle and cell-size control models for *Escherichia coli* and *Bacillus subtilis*. *Front. Microbiol.* **12**, 721899 (2021).
62. T. Hunt, A. Murray, *The Cell Cycle: An Introduction* (Oxford University Press, 1993).
63. S. M. Mangiameli, J. A. Cass, H. Merrikh, P. A. Wiggins, The bacterial replisome has factory-like localization. *Curr. Genet.* **64**, 1029–1036 (2018).
64. K. Gras, D. Fange, J. Elf, The *Escherichia coli* chromosome moves to the replisome. bioRxiv [Preprint] (2023). https://doi.org/10.1101/2023.07.12.548795 (Accessed 18 July 2024).
65. B. Youngren, H. J. Nielsen, S. Jun, S. Austin, The multifork *Escherichia coli* chromosome is a self-duplicating and self-segregating thermodynamic ring polymer. *Genes Dev.* **28**, 71–84 (2014).
66. D. Huang *et al*., The in vivo measurement of replication fork velocity and pausing by lag-time analysis. *Nat. Commun.* **14**, 1762 (2023).
67. F. G. Pflug, D. Bhat, S. Pigolotti, Genome Replication in Asynchronously Growing Microbial Populations. *PLoS Comput. Biol.* **20**, e1011753 (2024).
68. D. Bhat, S. Hauf, C. Plessy, Y. Yokobayashi, S. Pigolotti, Correction: Speed variations of bacterial replisomes. *eLife* **12**, e75884 (2023).
69. J. F. Pelletier *et al*., Genetic requirements for cell division in a genomically minimal cell. *Cell* **184**, 2430–2440.e16 (2021).
70. L. Olivi *et al*., Towards a synthetic cell cycle. *Nat. Commun.* **12**, 1–11 (2021).
71. D. J. Clark, O. Maaløe, DNA Replication and the Division Cycle in Escherichia Coli. *J. Mol. Biol.* **23**, 99–112 (1967).
72. F. C. Neidhardt, P. L. Bloch, D. F. Smith, Culture medium for enterobacteria. *J. Bacteriol.* **119**, 736–747 (1974).
73. M. S. Guyer, R. R. Reed, J. A. Steitz, K. B. Low, Identification of a sex-factor-affinity site in *E. coli* as gamma delta. *Cold Spring Harb. Symp. Quant. Biol.* **45**, 135–140 (1981).
74. J. H. Miller, *Experiments in Molecular Genetics* (Cold Spring Harbor Laboratory, 1972).
75. L. Riber *et al*., Hda-mediated inactivation of the DnaA protein and dnaA gene autoregulation act in concert to ensure homeostatic maintenance of the *Escherichia coli* chromosome. *Genes Dev.* **20**, 2121–2134 (2006).
76. J. Frimodt-Møller, G. Charbon, K. A. Krogfelt, A. Løbner-Olesen, Control regions for chromosome replication are conserved with respect to sequence and location among *Escherichia coli* strains. *Front. Microbiol.* **6**, 1011 (2015).
77. K. A. Datsenko, B. L. Wanner, One-step inactivation of chromosomal genes in *Escherichia coli* K-12 using PCR products. *Proc. Natl. Acad. Sci. U.S.A.* **97**, 6640–6645 (2000).
78. P. P. Cherepanov, W. Wackernagel, Gene disruption in *Escherichia coli*: TcR and KmR cassettes with the option of Flp-catalyzed excision of the antibiotic-resistance determinant. *Gene* **158**, 9–14 (1995).
79. R. Reyes-Lamothe, D. J. Sherratt, M. C. Leake, Stoichiometry and architecture of active DNA replication machinery in *Escherichia coli*. *Science* **328**, 498–501 (2010).
80. E. Balleza, J. M. Kim, P. Cluzel, Systematic characterization of maturation time of fluorescent proteins in living cells. *Nat. Methods* **15**, 47–51 (2018).
81. L. C. Thomason, J. A. Sawitzke, X. Li, N. Costantino, D. L. Court, Recombineering: Genetic engineering in bacteria using homologous recombination. *Curr. Protoc. Mol. Biol.* **106**, 1.16.1–1.16.39 (2014).
82. L. Riber *et al*., Hda-mediated inactivation of the DnaA protein and dnaA gene autoregulation act in concert to ensure homeostatic maintenance of the *Escherichia coli* chromosome. *Genes Dev.* **20**, 2121–2134 (2006).
83. A. Løbner-Olesen, K. Skarstad, F. G. Hansen, K. von Meyenburg, E. Boye, The DnaA protein determines the initiation mass of *Escherichia coli* K-12. *Cell* **57**, 881–889 (1989).
84. S. Taheri-Araghi *et al*., Cell-Size control and homeostasis in bacteria. *Curr. Biol.* **25**, 385–391 (2015).
85. R. Thiermann *et al*., Tools and Methods for High-Throughput Single-Cell Imaging with the Mother Machine. *eLife* **12**, RP88463 (2024).
86. O. Ronneberger, P. Fischer, T. Brox, "U-Net: Convolutional networks for biomedical image segmentation" in *Medical Image Computing and Computer-Assisted Intervention–MICCAI 2015* (Springer International Publishing, 2015), pp. 234–241.
87. H. Fu. Dispensability of extrinsic DnaA regulators in Escherichia coli cell-cycle control (raw data). Dryad. https://doi.org/10.5061/dryad.vq83bk42p. Accessed 19 July, 2024.